2018 BEAM-PARK OBSERVATIONS OF SPACE DEBRIS WITH THE EISCAT RADARS

J. Vierinen[(1)], D. Kastinen[(2)], J. Markkanen[(3)], T. Grydeland[(4)], J. Kero[(5)], A. Horstmann[(6)], S. Hesselbach[(6)], C. Kebschull[(6)], E. Røynestad[(1)], and H. Krag[(7)]

[(1)]*UiT - Arctic University of Norway, Postboks 6050 Langnes, 9037 Tromsø, Norway*
[(2)]*Swedish Institute of Space Physics (IRF), Box 812, 98128 Kiruna, Sweden, and Umeå University, Department of Physics, 90187 Umeå, Sweden*
[(3)]*EISCAT Scientific Association, Tähteläntie 62, 99600 Finland*
[(4)]*Northern Research Institute (Norut), Postboks 6434, 9294 Tromsø, Norway*
[(5)]*Swedish Institute of Space Physics (IRF), Box 812, 98128 Kiruna, Sweden*
[(6)]*Technical University of Braunschweig (TU-BS), Universitätsplatz 2, 38106 Braunschweig, Germany*
[(7)]*ESA ESOC Space Debris Office, Darmstadt, Germany*

ABSTRACT

Monitoring the evolution of the space debris environment requires regular radar observations of the space debris population. This study presents the results from 24 hours of beam-park observations of space objects conducted simultaneously with the EISCAT Svalbard and Tromsø radars on and between January 4th and 5th, 2018. The measurements are processed with a new matched filter bank analysis program, which doubles the coherent integration time, and hence sensitivity, compared with the previous program. We observe 2077 objects with the Tromsø radar and 2400 objects with the Svalbard radar. The detections are correlated with the NORAD catalog. We find that 68% of the Tromsø and 85% of the Svalbard radar detections are from objects in the NORAD catalog, with most of the catalog object detections being in the side lobes of the radar antenna. The beam-park data are compared with a simulated beam-park experiment for catalog objects. The simulation uses a radar detection model that includes the effects of coherent integration and an antenna beam shape with side lobes. We find that the simulation agrees well with the measurements, indicating that the radar sensor response is accurately modeled. Our results highlight the importance of modeling antenna side lobes when analyzing beam-park measurements. Not taking taking into account side lobe detections can lead to an underestimation of radar cross-sections and an overestimation of population density.

Keywords: Space debris; Beam-park observations; Space debris model validation.

1. INTRODUCTION

Beam-park radar observations with high power large aperture radars are an important source of information about the space object population. Such measurements can be used as a basis for estimating the statistical distribution of space objects [Kri14, FGW$^+$09] and to verify such models [SS97, BLM00, JK97]. The validity of space object population models have important implications on predictions of the long term evolution of the space object environment, and on the risks associated with space flight.

The high-latitude location of the EISCAT scientific association's high power large aperture radars means that objects in high inclination orbits pass within the field of view more often than they will for radars at lower latitudes. The EISCAT Svalbard radar [W$^+$97] is located at 78.15°N 16.02°E. The EISCAT Tromsø radar [RW85] is located at 69.58°N 19.23°E. Both of these radars can observe small objects down to a few centimeters in diameter [MLL05a, KKJ$^+$07] and have in the past been used to e.g., characterize the debris created by the Chinese anti-satellite event [MJK09, LCM12] and the Iridium-Cosmos collision [VMK09].

In order to assess the space debris population in 2018, we have conducted a 24 hour beam-park observation with the Svalbard and Tromsø radars simultaneously. In processing these measurements, we have made four improvements to our processing compared with previous observations: 1) We have doubled the signal-to-noise ratio (SNR) of detections by doubling the coherent integration time, 2) we have correlated the detections with the NORAD daily snapshot of the space object catalog, 3) we have employed an improved clustering algorithm for grouping together raw coherent integration measurements into detections, and 4) we have developed a radar sensor response that simulates the EISCAT beam-park measurement.

The EISCAT radars are primarily used for studies of the Earth's upper atmosphere, and therefore lack a monopulse feed. This makes it harder to ascertain the true direction to a target, without which it is impossible to obtain a measurement of its true radar cross-section. Many of the detections of larger objects during a beam-park experiment are often observed within the side lobes of the antenna beam. In order to model these effects for beam-park measurements, we have developed a new sensor model, which takes into account the random locations of objects within the radar beam and models the SNR distribution of the detections.

Catalog correlation allows for the identification of detections with known catalog objects. This provides a way to validate the radar sensor response, as the NORAD catalog objects have relatively well characterized radar cross-sections. Catalog correlation also helps when comparing the results of beam-park observations with space object population models for smaller sized objects, as it is to a significant extent possible filter out low SNR detections due to large objects in the radar antenna side lobes. This helps to avoid confusing detections due to large objects in the side lobes of the antenna with small objects near the on-axis position of the antenna.

In this study, we present the results from the 2018 EISCAT beam-park campaign. We have compared the results with a simulated beam-park observation for NORAD catalog objects, in order to validate the radar sensor model.

2. RADAR CONFIGURATION

The EISCAT UHF Tromsø and EISCAT Svalbard radars were used to perform a simultaneous 24 hour beam-park observation of space objects between between 2018-01-04T12:00 UTC and 2018-01-05T12:00 UTC. The radar mode on both radars was the standard EISCAT space object beam-park experiment, which utilizes 1920 μs binary phase coded long pulses with 30 μs baud length and 64 bauds per code. The interpulse period (IPP) was 20 ms. The program uses 128 unique transmit codes before repeating the cycle, which means that range aliasing only occurs after $3.8 \cdot 10^5$ km. The echoes and transmit pulses were recorded in complex baseband format with a 1 MHz sample-rate and analyzed off-line.

The Tromsø radar has an operating frequency of 930 MHz and used $\approx$ 1.6 MW of peak power for the experiment. The system noise temperature was $\approx$100 K. The Svalbard radar has an operating frequency of 500 MHz, ≈ 0.7 MW peak power and a system noise temperature of ≈ 100 K. Both radars were pointing towards the East with a 90° azimuth and 75° elevation angle above the horizon, which is well suited to observe objects in high inclination orbits as they transit on ascending or descending tracks. With this pointing direction, range-rate provides information about the inclinations of the detected objects.

The measurements were analyzed using a generalized matched filter (GMF), which is matched to range, radial range-rate, and radial acceleration [MLL05b]. We have implemented the algorithm on the Stallo supercomputer located at University of Tromsø. With the increased computing capacity, we have been able to coherently integrate 10 IPPs, which has doubled the sensitivity of the analysis compared to the previous program which coherently integrated five IPPs. The increase in sensitivity was confirmed by comparing the results with the previous analysis program results. The new analysis has on average twice the SNR.

The detection threshold for objects was: SNR higher than 25. This provides a relatively small false detection rate and has a nearly 100% probability of detection [KBKB$^+$00]. SNR for coherent integration based detection with 10 pulses of integration is:

$$\frac{S}{N} \approx \frac{P_{\mathrm{tx}} G^2 \sigma \lambda^2}{(4\pi)^3 R^4 k_B T \cdot 45}, \tag{1}$$

where P_{tx} is transmit power, G is gain, σ is the radar cross section, λ is wavelength, R is range, k_B is the Boltzmann constant, T is receiver noise temperature, and the term 45 is the effective noise bandwidth (Hz) for 10 pulses integrated together.

Another improvement to the signal processing is that we have applied a better algorithm for clustering detections [Vie13], which is based on Bayesian model selection and fitting of a radial trajectory to individial raw GMF measurements that are candidate detections. When comparing with previous observations, the path lengths of detections are significantly longer than with the previous method. This means that fewer detections in the antenna side-lobes are misclassified as weak detections or split into several detections. Clustering of raw measurements is demonstrated in Figure 1, which shows the output of the GMF as a function of range and time in units of SNR. In the Figure, a space object can be seen traversing through the side-lobes of the radar antenna. There is a gap of about seven seconds between the first detection of the object and when it reappears, which is due to a spurious side-lobe. Such sidelobes, which deviate from the theoretical beam pattern, exist in all antenna systems and are caused by slight imperfections in the antenna geometry. They can also correspond to contributions from e.g., antenna supports [Lam89].

3. SENSOR RESPONSE MODEL

In order to interpret our results, we have developed a sensor model that allows us to simulate a beam-park measurement, provided with a population of objects. The sensor response model takes into account the radar transmit power, receiver noise power, coherent integration length, antenna beam pattern, pointing direction, and location of the radar. The model also takes into account the size of the object, and its orbital elements. The sensor model has been implemented as part of the Space Object

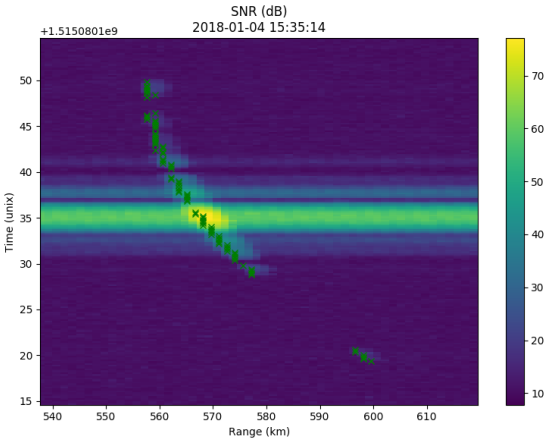

Figure 1. Example detection of a high SNR radar target, which can be observed traversing through many sidelobes. The detection lasts for 30 seconds. There is also a 7 second gap in between measurements after the object is first seen and when it is seen again. This is due to a detection in a spurious sidelobe. Green crosses indicate raw GMF measurements that are grouped together as one single detection based on a radial trajectory model fit.

Radar Tracking Simulator (SORTS), which is discussed in a companion paper [KVK+19]. The model is similar to PROOF [KBKB+00], but with coherent integration based detection and including contributions of the side lobes of the radar antenna.

We assume the object to have a radar cross-section that corresponds to a perfectly conducting sphere of a certain diameter, which is either in Rayleigh or optical scattering regime. This is the standard scattering model used for modeling the radar cross-section of space debris [SS97, KBKB+00].

The sensor model takes into account antenna side lobe contributions. This is important, as a significant portion of large radar-cross-section object detections occur within the side lobes of the antenna beam. This is the case for any high power large aperture radar system. Side lobes have a larger geometric collecting area than the main lobe, albeit with reduced sensitivity. Often, this reduced sensitivity is not sufficient to exclude detections of an object. Therefore, high RCS objects can be a large contribution to the overall number of detections.

We have used a Cassegrain antenna aperture model for the Svalbard and Tromsø radars, which includes effects of the main reflector and aperture blockage due to the subreflector and antenna support struts. The beam pattern is modeled to be axially symmetric. The beam pattern is based on the measured Tromsø radar beam shape. The Svalbard beam pattern is based on the measured Tromsø beam pattern, but scaled in angle based on frequency and in power by peak gain. The measurements only extend up to 5 degrees off axis, after which the gain is tapered to a constant -50 dB. The one-way gain model used for the Tromsø and Svalbard radar sensor models is shown

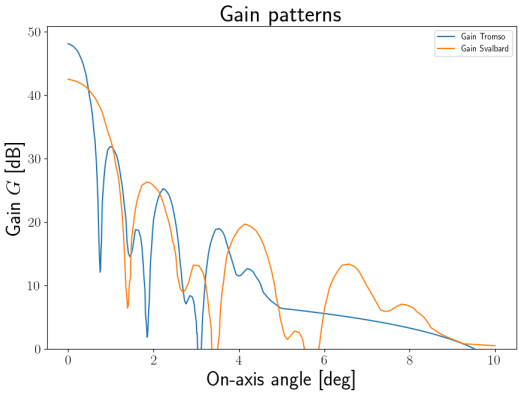

Figure 2. Beam pattern models for the Svalbard and Tromsø radars. The model is based on the measured Tromsø radar beam pattern up to 5 degrees, and tapered to -50 dB for larger angles. The Svalbard beam pattern model is scaled by wavelength and based on the Tromsø antenna beam pattern.

in Figure 2.

We have combined the radar sensor model with a space object population generated using the latest development version of the MASTER model [FGW+09] to allow simulating beam-park measurements. Each object in the population model is associated with the orbital elements, size, and mass. We randomize the mean anomaly (position along orbit) uniformly with a random number between 0 and 2π for each beam-park simulation. Objects are propagated using the SGP4 propagator [VC08]. We obtain simulated detections by calculating the SNR of each object along its track and reporting detections that exceed the detection threshold. We include the true antenna gain from the position of the object relative to the on-axis position of the radar antenna.

The NORAD catalog is part of the MASTER model, and represents a well calibrated subset of the model. Because the sensor model uses a random mean anomaly for each object, the NORAD catalog objects in the model do not correspond to the true NORAD catalog, but will have a similar statistical distribution of orbital elements and sizes.

Because the latest version of the MASTER model is not yet released, we only used the portion of the model that corresponds to NORAD catalog objects. The primary goal for this study is to verify that the radar sensor model agrees with the well known portion of the space object population. This can readily be done, by comparing NORAD catalog correlated beam-park measurements with a simulated beam-park observation.

We will refer to the simulated measurements obtained by combining the radar sensor model with the NORAD catalog population with "model" in the results shown later on. We will refer to the portion of the model that determines the radar detection of an object as the "radar sensor

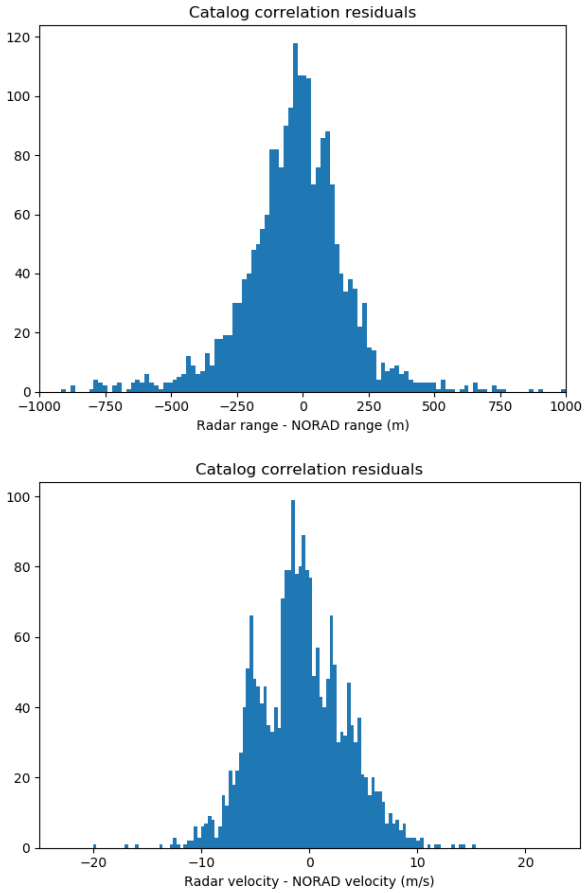

Figure 3. Range and range-rate residuals between beam-park detections and NORAD catalog objects for the Svalbard radar. We only show objects that have been correlated with the catalog.

response model".

4. CATALOG CORRELATION

In order to correlate the beam-park detections with the NORAD catalog, we use the the daily snapshot of two-line elements for the day of observations. The objects are propagated using SGP4 to determine the range and radial range-rate of objects. Range and radial range-rate residuals between the catalog predictions and the detected range and radial range-rate are used to determine if a detected object is a catalog object. We have used a threshold of < 1 km range residual and < 20 m/s radial range-rate residual as a criteria for associating a detection with a catalog object. Figure 4 shows the range and radial range-rate residuals for all of the correlated objects for the Svalbard radar. The distribution of residuals are similar for the Tromsø radar. Note that we have not used a high resolution analysis for range and radial range-rate, so the true residuals can be smaller than this.

Out of the 2400 detections obtained with the Svalbard

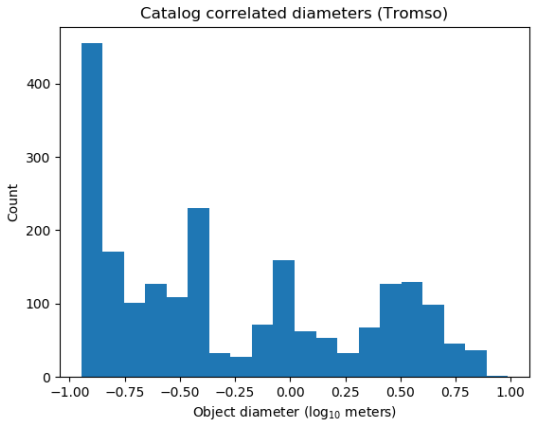

Figure 4. Diameters of NORAD catalog correlated objects in Tromsø based on the beam park simulation.

radar, 2043 could be correlated with objects in the NORAD catalog (85%). Out of the 2077 detections obtained with the Tromsø radar, 1411 could be correlated with objects in the NORAD catalog (68%). The explanation for such a large number of catalog objects is that the Svalbard and Tromsø radars use a relatively long wavelength (0.6 and 0.32 meters). Most of the objects that are not in the catalog are significantly smaller than the radar wavelength and are in the Rayleigh scattering regime. This makes the radars less sensitive to small non-catalog objects. Also, catalog objects typically have a very large radar cross-section, allowing them to be detected far into the side lobes of the radar antenna.

The simulation of a beam-park measurement based on the NORAD catalog objects produced 2325 catalog object detections for the Svalbard radar and 1329 catalog object detections for the Tromsø radar. The simulation produced 12% more catalog detections for the Svalbard radar than we observed. For the Tromsø radar, the simulation produced 6% less catalog detections than we observed. These are very close to the number of actual detections of catalog objects and indicates that the sensor model is reasonably accurate for larger objects. While our beam-park simulation includes the orbital elements and sizes of the NORAD catalog objects, the mean anomaly of each object is random. Therefore, we would not expect the sensor model to exactly match the observations. However, we would expect a similar number of detections, and a similar distribution of all observable parameters: range, radial range-rate, SNR, and time of day.

5. BEAM-PARK RESULTS

The left hand side of Figure 5 shows detections as a function of time and range for the Tromsø and Svalbard radars. Each object correlated with the NORAD catalog is shown with blue and each object not within the catalog is shown in red. The right hand side of the Figure 5

shows simulated beam-park detections based on the NORAD catalog and the radar sensor response model. The general features of the measurements agree well with the simulated measurement.

The left hand side of Figure 6 shows detections as a function of Doppler velocity and range for the Tromsø and Svalbard radars. Again, each object correlated with the NORAD catalog is shown with blue and each object not within the catalog is shown in red. The right hand side of Figure 6 shows simulated detections using only the NORAD catalog as the population. The general features of the beam-park measurement and the simulated measurement agree relatively well for both radars. The detections are clustered at similar radial range-rates and ranges as the model predicts.

One interesting feature of the measurements is a cluster of detections that can be seen in the Svalbard measurements at range 1300 km at 22.5 hours. This cluster primarily consists of objects not in the NORAD catalog (red color). The Tromsø measurement also shows a cluster of detections at 22.5 hours at a similar altitude. The same cluster can also be seen in the radial range-rate vs range plot shown in Figure 6 at $\approx \pm 0.3$ km/s. This cluster could be associated with further fragmentation of the SNAP-10A nuclear powered spacecraft [JMR67], which has been reported previously by Stokely and Stansbery [SS08].

In order to assess the validity of the radar sensor response portion of our model, we have compared the portion of objects that are determined as objects within the NORAD catalog with simulated detections for catalog objects. We have separated the catalog objects and non-catalog objects in the histograms showing the distributions of range, range-rate, and SNR of observations. This allows us to separately evaluate the validity of the full model and to see the distribution of non-catalog objects.

Figure 7 shows histograms of detections as a function of range, radial range-rate, time of day, and SNR. The left hand side panels shows the histograms for the Tromsø radar and the right hand side shows the same results for the Svalbard radar. The line labeled " model" (green line) shows the histogram for the portion of the model that corresponds to NORAD catalog objects. The histograms for the beam-park measurements are separated into catalog correlated detections (blue) and non-catalog detections (orange). The model and catalog correlated detection histograms for range, radial range-rate, and time of day agree reasobly well with one another. The SNR histogram agrees reasonably well for Tromsø.

For Svalbard, the SNR histogram agrees, but has more discrepency between the model and the measurements. This is probably due to a less accurate antenna gain model. We do not have a measurement of the Svalbard radar antenna beam pattern, so we have used a scaled version of the Tromsø antenna beam pattern in our radar sensor response model. Both antennas are similar Cassegrain antennas of the same size, so their beam patterns should be somewhat close. The main discrepancies in the SNR histogram for Svalbard occur at 35 dB and 25 dB. At 35 dB, the model predicts more detections than are observed, and at 25 dB, the model predicts less detections than are observed. The reason for this could be that we have overestimated the gain of the first of second side lobe of the antenna in our model. This also could be a result of an axial asymmetries in the beam pattern, which would result in a smoother SNR histogram.

6. DISCUSSION

It is extremely difficult to construct an antenna that has peak far side lobes much less than 40 dB below the peak on-axis gain [Lam89, MP75]. Spurious side lobes can be significantly higher than this. Consider a side lobe with -30 dB gain relative to the on-axis gain. This will result in a two way reduction of -60 dB in SNR. This will still leave a 20 dB SNR for objects that have a peak SNR of 80 dB on axis. Larger satellites will easily produce a peak SNR of this magnitude when on-axis for the EISCAT radars. Thus, it is not surprising that large space objects be detected quite far from the on-axis position of a high gain radar antenna.

The first and second side lobes of the EISCAT antennas are only about 16 and 22 dB lower than the peak on-axis gain of the antenna, which means that larger objects can easily be detected there. An example of detections within the side lobes with the Svalbard radar is shown in Figure 1. A high RCS object can be seen traversing a spurious side lobe, as well as several side lobes near the main lobe. The object most likely crosses the main lobe of the antenna in this case. This is a very typical detection for a larger object with the EISCAT radars, with the exception that detections of larger objects often do not cross the main lobe of the antenna beam.

When modeling beam-park measurements of space objects, the contributions of detections in antenna side lobes need to be addressed, as they can contribute to a significant fraction of the detections. In our case, we found that over half of the beam-park detections are due to large NORAD catalog objects. If modeling of the side lobe contributions is not done properly, there is a significant risk of over-estimating the amount of small sized debris, because a large object detected in an antenna beam side lobe may be interpreted as a small object in the main lobe of the beam. Correlating for the NORAD catalog and removing catalog objects from beam-park measurements will alleviate this problem to some extent, but there are a significant number of large objects not in the NORAD catalog.

The importance of modeling side lobe detections with high power large aperture radars has been identified for interpreting meteor head echoes [VFM14]. Mitchell et.al., [MDJ$^+$18] recently found using simultaneous optical and radar measurements with Arecibo radar that only a small fraction of the simultaneous detections of meteor head echoes were determined to be in the main lobe of the

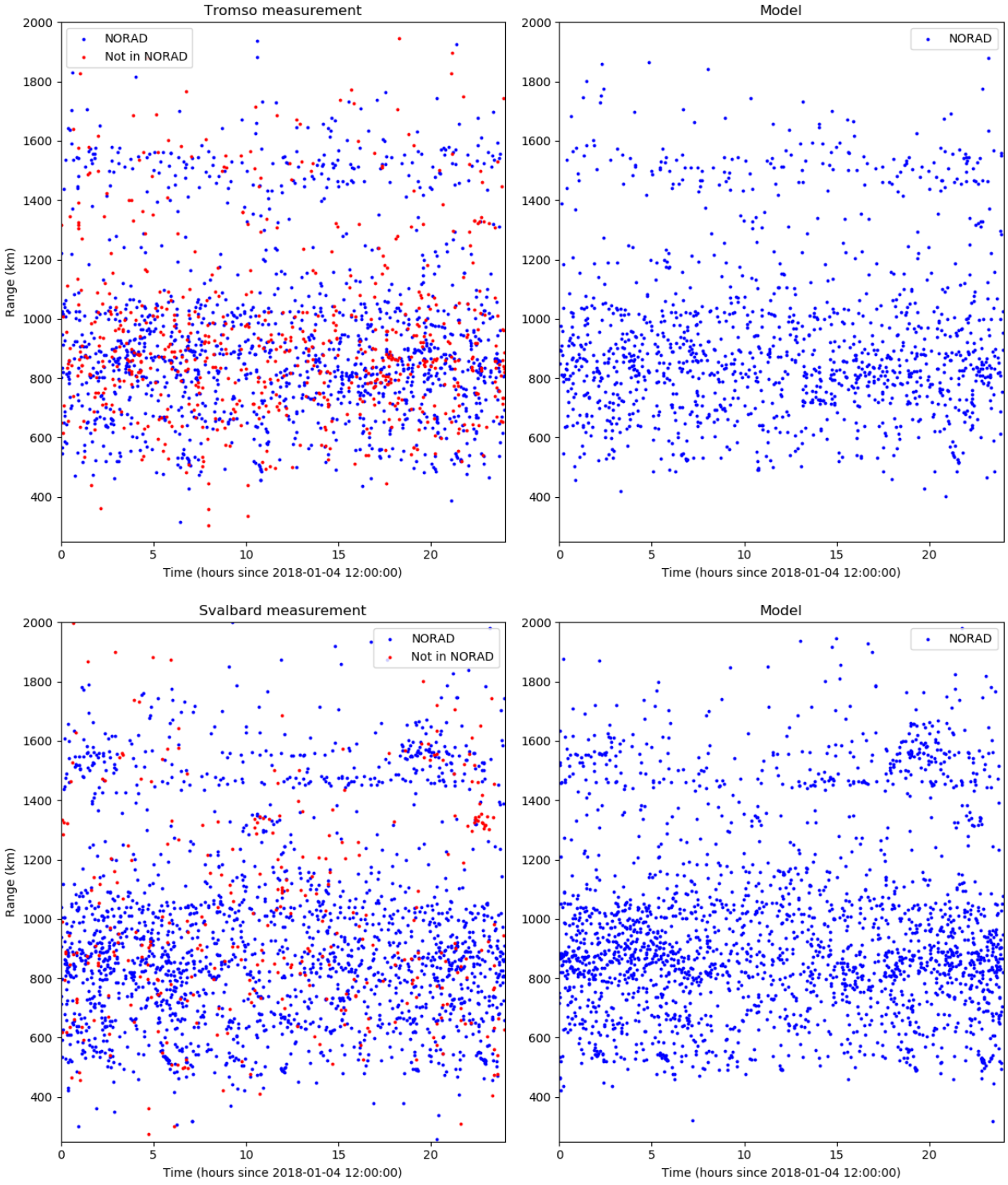

Figure 5. Detections as a function of time and range for the Svalbard and Tromsø radars. Left: detections from the beam-park campaign, Right: Simulated detections for NORAD objects only.

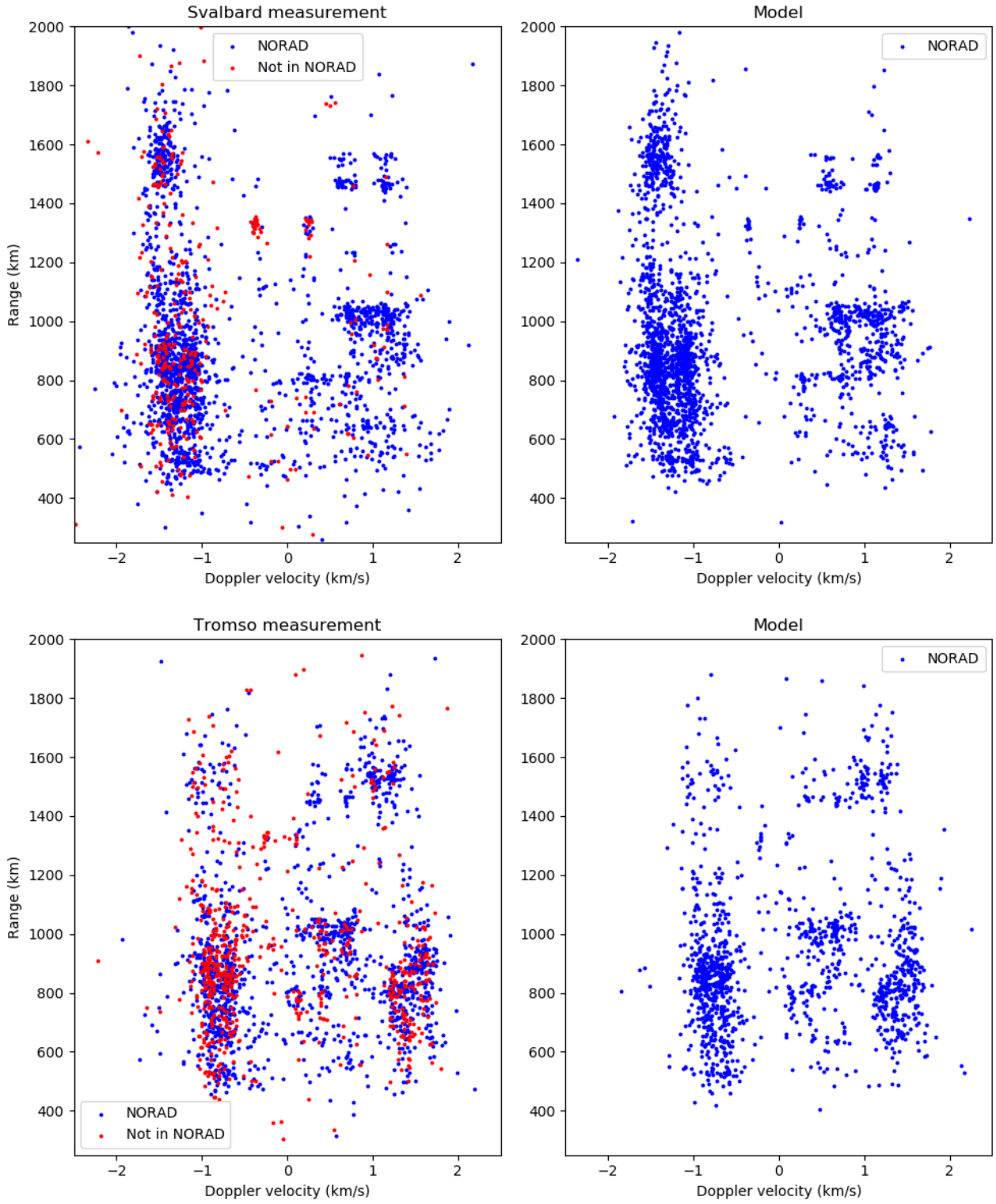

Figure 6. Top left: Radial range-rate vs Range of detections for the Svalbard radar. Top right: Simulated beam-park detections for Svalbard using NORAD catalog objects only. Bottom left: Radial range-rate vs Range of detections for the Tromsø radar. Bottom right: Simulated beam-park detections for Tromsø using NORAD catalog objects only.

Figure 7. Histograms of detections for Tromsø (left) and Svalbard (right). Top: range histogram, second from top:

radar antenna. A significant fraction of detections were found to be in the far side lobes of the antenna, beyond the first side lobe. These findings imply that the radar-cross-sections of meteor head echoes measured previously using Arecibo have been previously greatly underestimated, given the smaller backscattered powers received in the side lobes. These findings are relevant for space object observations, as meteor head echoes are also high RCS radar targets, which have a very similar range of SNRs.

In order to verify our radar sensor model for the EISCAT radars, we have simulated a beam-park measurement using the NORAD population. We have randomized the mean anomalies of each object in the model, in order for the model to be similar to the NORAD catalog in terms of the distribution of orbital elements and object sizes. A simulated beam-park measurement using this model produces a similar distribution of observables as the NORAD correlated beam-park detections. Most importantly, the simulated beam-park measurement has nearly the same distribution of SNRs as our observation. This indicates that the radar sensor reponse model is applicable for simulating of EISCAT beam-park measurements for larger objects. This does not conclusively prove that the model is valid for smaller objects, but provides some level of confidence that the model should also work for smaller objects.

There are several differences between the new beam-park observations compared with previous EISCAT measurements, which are significant when comparing the beam-park observations to debris models: 1) we have doubled the sensitivity of the coherent integration analysis, detecting weaker echoes, 2) we have correlated measurements with the NORAD catalog, which allows identifying detections that do not correspond to catalog objects, and 3) we have employed an improved clustering algorithm, which combines raw range, range-rate, and acceleration measurements from the GMF output into individual detections. The new clustering algorithm produces longer track lengths than before. These improvements have potentially reduced the number of antenna side lobe detections that are misclassified as weak objects in the main lobe.

7. CONCLUSIONS

We have presented beam-park observations performed in early 2018 with an improved measurement analysis. In order to proceed with the interpretation of these results, we have developed a radar sensor response model for the EISCAT radars and validated it against the well characterized NORAD catalog objects. We find using a simulated beam-park measurement that the radar sensor response model is in good agreement with our beam-park observations. This indicates that the model is applicable to at least larger > 10 cm diameter objects. Using this model to estimate the distribution of smaller non-catalog objects from EISCAT beam-park measurements is a topic of future work.

Our results highlight the importance of modeling the full beam pattern of the radar system when comparing beam-park observations with space object population models. Larger objects can easily be detected relatively far away off-axis due to large radar cross-section. We expect this effect to be present in all high power large aperture systems. Not taking this into account may lead to a significant overestimation of the density of objects when beam-park measurements are used to validate space object population models.

ACKNOWLEDGMENTS

Juha Vierinen would like to acknowledge the support of the Tromsø Science Foundation for this work. The work is also supported by ESA through the AO9062 EISCAT 3D Performance Analysis project.

EISCAT is an international association supported by research organisations in China (CRIRP), Finland (SA), Japan (NIPR and STEL), Norway (NFR), Sweden (VR), and the United Kingdom (NERC)

REFERENCES

BLM00. D Banka, L Leushacke, and D Mehrholz. Beam-park-experiment-1/2000 with TIRA. *Space Debris*, 2(2):83–96, 2000.

FGW+09. S Flegel, J Gelhaus, C Wiedemann, P Vorsmann, M Oswald, S Stabroth, H Klinkrad, and H Krag. The MASTER-2009 space debris environment model. In *Fifth European Conference on Space Debris*, volume 672, 2009.

JK97. R Jehn and H Klinkrad. From measurement results to space debris environment models. In *IAF, International Astronautical Congress, 48 th, Turin, Italy*, 1997.

JMR67. Richard A Johnson, William T Morgan, and Sol R Rocklin. Design, ground test and flight test of snap 10a, first reactor in space. *Nuclear engineering and design*, 5(1):7–21, 1967.

KBKB+00. H Krag, P Beltrami-Karlezi, J Bendisch, H Klinkrad, D Rex, J Rosebrock, and T Schildknecht. PROOF - The extension of ESA's MASTER Model to predict debris detections. *Acta Astronautica*, 47(2-9):687–697, 2000.

KKJ+07. Holger Krag, Heiner Klinkrad, Rüdiger Jehn, Jussi Markkanen, and Ludger Leushacke. Detection of small-size space debris with the fgan and eiscat radars. In *Proc. 7th US-Russian Space Surveillance Workshop*, 2007.

Kri14. Paula H Krisko. The new NASA orbital debris engineering model ORDEM 3.0. In *AIAA/AAS Astrodynamics Specialist Conference*, page 4227, 2014.

KVK+19. Daniel Kastinen, Juha Vierinen, Johan Kero, Sebastian Hesselbach, Grydeland Tom, and Holger Krag. Next-generation space object radar tracking simulator: SORTS++. 2019.

Lam89. James Lamb. Far-out sidelobes in large reflector antennas. Technical report, Green Bank Telescope Memo 13, 1989.

LCM12. Alan Li, S Close, and J Markannen. EISCAT Space Debris after the International Polar Year (IPY). In *Conference Proceedings from IAC*, volume 12, page A6, 2012.

MDJ+18. RG Michell, M DeLuca, D Janches, R Chen, and M Samara. Simultaneous optical and dual-frequency radar observations of small mass meteors at arecibo. *Planetary and Space Science*, 2018.

MJK09. J Markkanen, R Jehn, and H Krag. Eiscat space debris during the ipya 5000 hour campaign. In *Proc. 5th ESA space debris conference*, 2009.

MLL05a. Jussi Markkanen, Markku Lehtinen, and M Landgraf. Real-time space debris monitoring with EISCAT. *Advances in space research*, 35(7):1197–1209, 2005.

MLL05b. Jussi Markkanen, Markku Lehtinen, and M Landgraf. Real-time space debris monitoring with EISCAT. *Advances in space research*, 35(7):1197–1209, 2005.

MP75. C Mentzer and L Peters. A gtd analysis of the far-out sidelobes of cassegrain antennas. *IEEE Transactions on Antennas and Propagation*, 23(5):702–709, 1975.

RW85. H Rishbeth and PJS Williams. The EISCAT ionospheric radar-The system and its early results. *Quarterly Journal of the Royal Astronomical Society*, 26:478–512, 1985.

SS97. E Stansbery and T Settecerri. A comparison of Haystack and HAX measurements of the orbital debris environment. In *Second European Conference on Space Debris*, volume 393, page 59, 1997.

SS08. CL Stokely and EG Stansbery. Identification of a debris cloud from the nuclear powered snapshot satellite with haystack radar measurements. *Advances in Space Research*, 41(7):1004–1009, 2008.

VC08. David Vallado and Paul Crawford. Sgp4 orbit determination. In *AIAA/AAS Astrodynamics Specialist Conference and Exhibit*, page 6770, 2008.

VFM14. J Vierinen, J Fentzke, and E Miller. An explanation for observations of apparently high-altitude meteors. *Monthly Notices of the Royal Astronomical Society*, 438(3):2406–2412, 2014.

Vie13. Juha Vierinen. Methods and arrangements for detecting weak signals, US Patent 8,463,579, 2013.

VMK09. Juha Vierinen, Jussi Markkanen, and Holger Krag. High power large aperture radar observations of the iridium-cosmos collision. In *Proc. 5th ESA space debris conference*, 2009.

W+97. G. Wannberg et al. The EISCAT Svalbard radar: A case study in modern incoherent scatter radar system design. *Radio Science*, 32(6):2283–2307, 1997.